View Article Online / Journal Homepage / Table of Contents for this issue
Dynamic Article Links

Journal of Materials Chemistry

Cite this: *J. Mater. Chem.*, 2012, **22**, 6856

www.rsc.org/materials

PAPER

Aluminium-doped n-type ZnS nanowires as high-performance UV and humidity sensors†

Peng Jiang,[a] Jiansheng Jie,*[b] Yongqiang Yu,[a] Zhi Wang,[a] Chao Xie,[a] Xiwei Zhang,[b] Chunyan Wu,[a] Li Wang,[a] Zhifeng Zhu[a] and Linbao Luo[a]

Received 21st October 2011, Accepted 20th January 2012
DOI: 10.1039/c2jm15365c

Published on 28 February 2012. Downloaded by HeFei University of Technology on 18/10/2015 13:13:38.

Controlling the electrical transport properties of II–VI nanostructures is vital to their practical applications. Here, we report the synthesis of n-type ZnS nanowires (NWs) by using aluminium (Al) as a dopant *via* a simple thermal co-evaporation method. The conductivities of the ZnS:Al NWs were greatly enhanced upon Al doping and could be further tuned in a wide range of 3 orders of magnitude by adjusting the doping level. Field-effect transistors (FETs) fabricated from individual ZnS:Al NWs revealed an electron concentration up to 1.3×10^{18} cm^{-3} in the NWs. Significantly, the doped NWs showed great potential as visible-blind UV sensors with an extremely high responsivity of 4.7×10^6 A W^{-1}, giving rise to a large gain-bandwidth (GB) of ~0.1 GHz. The high sensitivity of the ZnS:Al NWs to humidity was also investigated; the devices displayed a resistance variation of about 2 orders of magnitude in the relative humidity (RH) range of 50–90%. Our results demonstrate that the n-type ZnS:Al NWs have important applications in nanoelectronic and nano-optoelectronic devices.

I. Introduction

One-dimensional (1D) II–VI group semiconductor nanostructures have attracted extensive attention due to their tremendous potential in new-generation nanoelectronics and nano-optoelectronics.[1] Zinc sulfide (ZnS) is one of the most important II–VI compound semiconductors with a direct band gap of 3.7 eV and a large exaction binding energy of 40 meV. It has been widely used in light emitting diodes (LEDs), flat panel displays, injection lasers, infrared windows, and ultraviolet (UV) sensors.[2–4] Up to now, various ZnS nanostructures, including nanowires (NWs),[2] nanoribbons (NRs),[3] nanotubes (NTs),[4] and nanohelices,[5] have been successfully synthesized and their unique optical properties are intensively investigated.[6] Also, many efforts were devoted to explore their applications in diverse devices, such as field emitters,[7] and UV,[8,9] biologic,[10,11] and gas sensors.[12]

Owing to the distinct characteristics such as a wide band gap in the UV regime, high crystallinity, and high quantum efficiency, ZnS nanostructures are promising candidates for high-performance UV sensor applications. However, in contrast to other wide band gap materials such as ZnO and GaN NWs,[13,14] intrinsic ZnS nanostructures usually suffer from the high resistive nature and exhibit low sensitivity to the UV light. On the other hand, humidity sensors also have important applications in semiconductor electronics, environments, and agriculture and food processing industries. Although a variety of semiconductor nanostructures including carbon NTs, metal oxide nanoparticles, and SnO_2 NWs have been utilized in this field,[15,16] humidity sensors based on ZnS nanostructures are rarely studied. Therefore, it remains a challenge to achieve high-performance ZnS nano-sensors for future nanoelectronic and nano-optoelectronic applications.

Doping to the semiconductor nanostructures has been demonstrated to be a feasible method to tune their optoelectronic properties and further enhance their device performances.[17] Nevertheless, efficient doping in II–VI nanostructures is still hampered by the serious self-compensation effect and few reports have addressed this issue so far. Recently, Yuan *et al.* reported the synthesis of p-type ZnS NRs by using NH_3 as the dopant.[18] We also fabricated the high-performance Schottky barrier diodes based on Sb-doped ZnS NRs with controlled p-type conductivity.[19] Surface induced negative photoresponse was observed in the Bi-doped p-type ZnSe NWs.[20] In contrast, n-type ZnS nanostructures are less reported and further investigations are much demanded to promote their advanced applications in p–n homojunctions, superlattices, complementary circuitries and so on.

In this work, we exploit the potential applications of the ZnS nanostructures as high-performance nano-sensors. Controlled

[a] *School of Electronic Science and Applied Physics, Hefei University of Technology, Hefei Anhui 230009, P. R. China*
[b] *Institute of Functional Nano & Soft Materials (FUNSOM) and Jiangsu Key Laboratory for Carbon-Based Functional Materials & Devices, Soochow University, Suzhou Jiangsu 215123, P. R. China. E-mail: jason.jsjie@gmail.com*

† Electronic supplementary information (ESI) available. See DOI: 10.1039/c2jm15365c

 This journal is © The Royal Society of Chemistry 2012

View Article Online

Published on 28 February 2012. Downloaded by HeFei University of Technology on 18/10/2015 13:13:38.

n-type doping to the ZnS NWs was first accomplished by using aluminium (Al) as a dopant. High-sensitive and visible-blind UV sensors as well as humidity sensors were constructed, revealing the promising applications of the ZnS:Al NWs in new-generation nanoelectronics and nano-optoelectronics.

II. Experimental details

Synthesis of the Al-doped ZnS NWs was carried out in a horizontal tube furnace *via* a thermal co-evaporation method. Briefly, 0.3 g ZnS powder (Aldrich, 99.99%) was first loaded into an alumina boat and then transferred to the center position of the furnace. Another boat loaded with Al powder (Aldrich, 99.99%) served as the dopant and was placed near the ZnS source in the downstream direction. Si growth substrates were ultrasonically cleaned in acetone and ethanol for 15 min, respectively, and coated with 10 nm gold catalyst. The substrates were placed at the downstream ~10 cm from the Al source. After evacuating to a base pressure of 4×10^{-4} Pa, the reaction chamber was cleaned and filled with H_2 (5% in Ar) gas at a constant flow ratio of 50 sccm and the pressure was adjusted to 150 Torr. Afterwards, ZnS powder, Al powder, and Si substrates were heated to 1040 °C, ~950 °C, and ~600 °C, respectively, in one hour and maintained at those temperatures for one hour. After reaction, a layer of white wool-like product could be observed on the Si substrate surfaces. In order to control the transport properties of the ZnS NWs, three samples with varied Al doping levels were synthesized, labeled as AZ1, AZ2, and AZ3, corresponding to the molar ratio of ZnS:Al of 12 : 1, 10 : 1, and 5 : 1, respectively. Undoped ZnS NWs were also synthesized under the same conditions except an Al source was not used for comparison.

Morphologies and structures of the Al-doped ZnS NWs were characterized by field-emission scanning electron microscopy (FESEM, SIRION 200 FEG), X-ray diffraction (XRD, RigakuD/Max-γB, with Cu Kα radiation), and high-resolution transmission electron microscopy (HRTEM, Philips CM200 FEG). Compositions were analyzed by energy-dispersive X-ray spectroscopy (EDX, attached to the SEM), and X-ray photoelectron spectroscopy (XPS, Themo ESCALAB 250). Photoluminescence (PL) spectra were measured by using a He–Cd 325 nm laser as the excitation source (LabRAM-HR).

To evaluate the electrical properties of the Al-doped ZnS NWs, the NWs were first dispersed onto the oxidized p^+-Si substrate (300 nm SiO_2) at a desired density, and then indium tin oxide (ITO) electrodes were deposited on the NWs by using a pulsed laser deposition (PLD) system with KrF excimer laser (Lambda Physik COMPexPro 102, 248 nm, 120 mJ, 5 Hz) under the assistance of a mesh-grid mask composed of tungsten wires (5 μm in diameter). A fast annealing process in vacuum (5×10^{-4} Torr) at 300 °C for 3 min was carried out to further improve the electrical contact between the ITO electrodes and the ZnS:Al NWs. Electrical measurements were conducted on a semiconductor characterization system (Keithley 4200-SCS). Photoconductive properties of the ZnS:Al NWs were detected by using a monochromatic light source composed of a xenon lamp (150 W) and a monochromator (Omni-λ300). A mechanical chopper was used to generate pulsed incident light with frequency in the range of 0–400 Hz. The properties of the ZnS:Al NW humidity sensor were measured by using a home-built humidity detection system with 30% to 90% relative humidity (RH).

III. Results and discussion

Fig. 1a shows a typical FESEM image of the as-synthesized ZnS:Al NWs. It is seen that the NWs have diameter in the range of 20–150 nm and length of typically tens of micrometres. EDX profile of AZ2 also demonstrates that the NWs consist of only Zn and S elements in a roughly 1 : 1 ratio (inset in Fig. 1a). In addition, no trace of Al could be detected in the XPS spectrum of the ZnS:Al NWs (AZ3) (ESI, Fig. S1†), implying that the Al doping concentration was less than the detection limitation of XPS (1–5%). The HRTEM image and corresponding fast Fourier transform (FFT) pattern are depicted in Fig. 1b, revealing that the NWs are single crystalline with wurtzite structure. The growth orientation of the NWs is deduced to be $[10\bar{1}0]$. Fig. 1c displays the XRD patterns of both the doped and undoped ZnS NWs. All the diffraction peaks could be properly assigned to wurtzite phase ZnS and there is no obvious peak shift for the doped samples, indicating the high phase purity of the NWs and meantime the small lattice deformation caused by the Al incorporation. PL spectrum of the ZnS:Al NWs (AZ2) at room temperature shows two emission bands (Fig. 1d). The UV emission peak at ~336 nm corresponds to the near-band-edge (NBE) emission of ZnS, while the emission band at ~530 nm comes from the deep-level emission associated with the sulfur vacancies.[21] The peak positions and widths of the ZnS:Al NWs are nearly identical to the undoped ones except the increase of the defect emission intensity, indicating that the crystalline quality and structural integrity of the ZnS:Al NWs are not significantly degraded by Al incorporation. On the other hand, a new emission band originated from the donor–acceptor pair (DAP) transition from isolated Al donors to the acceptor states appears in the low temperature PL spectra (ESI, Fig. S2†),[21] which is indirect evidence for the successful Al doping in the ZnS NWs.

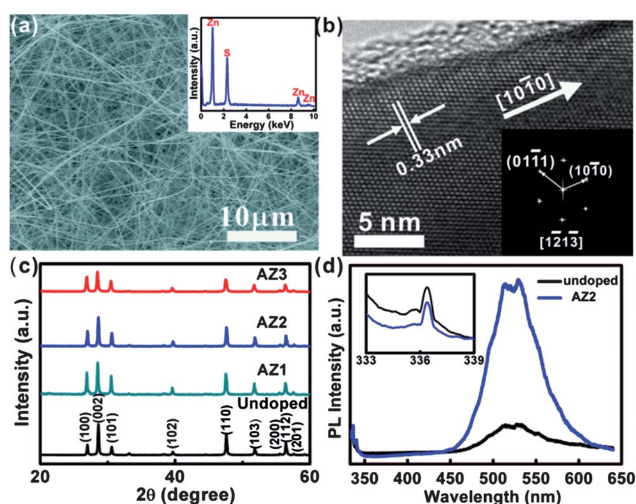

Fig. 1 (a) A typical FESEM image of the ZnS:Al NWs. Inset shows the corresponding EDX spectrum. (b) HRTEM image of the ZnS:Al NWs. Inset shows the corresponding FFT pattern. (c) XRD patterns of both the undoped and Al-doped ZnS NWs. (d) Room-temperature PL spectra of the undoped and Al-doped ZnS NWs (AZ2).

View Article Online

Published on 28 February 2012. Downloaded by HeFei University of Technology on 18/10/2015 13:13:38.

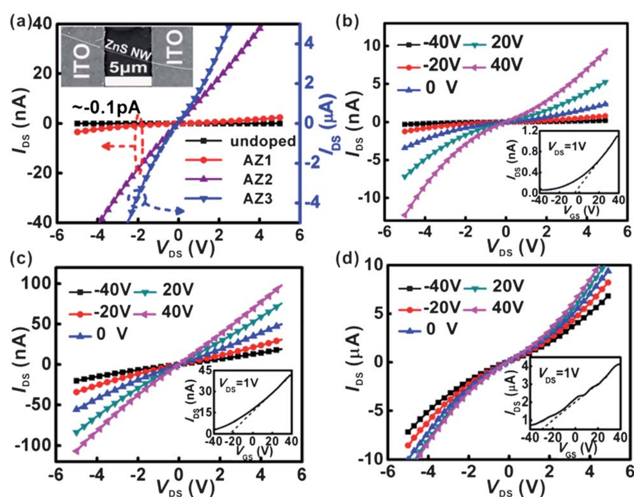

Fig. 2 (a) Typical I–V curves of both the undoped and Al-doped ZnS NWs with varied doping levels. Inset shows the representative FESEM image of the device based on a single NW. Electrical transfer characteristics of the ZnS:Al NWs with varied doping levels of (b) AZ1, (c) AZ2, and (d) AZ3. I_{DS}–V_{DS} curves were measured at varied V_{GS} ranging from −40 V to +40 V. Insets show the corresponding I_{DS}–V_{GS} curves at V_{DS} = +1 V.

The influence of Al doping on the transport properties of the ZnS NWs was assessed by the electrical measurements on an individual NW, as shown in Fig. 2. We note that the use of the ITO electrodes in this work is important to obtain the ohmic contact with the n-type ZnS:Al NWs (ESI, Fig. S3†). The detailed reason could be ascribed to the formation of a highly conductive interfacial oxide layer between ITO and the NWs. By this means the surface Fermi level pinning of the NWs could be eliminated, thus giving rise to a more efficient carrier injection from ITO to the NWs. From the typical I–V curves of the samples (Fig. 2a), it is found that the undoped ZnS NW exhibits an extremely low conduction current at the same level of noise (∼0.1 pA). Its conductivity is estimated to be as low as $\sim 10^{-8}$ S cm^{-1}. In contrast, a substantial enhancement in the conductivity is observed for the ZnS:Al NWs. The conductivities increase dramatically to 1.5×10^{-3}, 2.4×10^{-2}, and 3.9 S cm^{-1} for AZ1, AZ2, and AZ3, respectively. Fig. 2b–d display the representative source–drain current (I_{DS}) *versus* source–drain voltage (V_{DS}) curves of the doped samples measured at varied gate voltages (V_{GS}) ranging from −40 to +40 V in a step of +20 V. The I_{DS}–V_{GS} curves are also shown in the insets. It is obvious that all the ZnS NWs with varied doping levels exhibit pronounced gating effects and I_{DS} increases monotonously with increasing V_{GS}. This device feature is consistent with the typical behavior of a n-channel FET, thus certifying the n-type nature of the ZnS:Al NWs. The substitutional doping of Al^{3+} ions into the NW's lattice by replacing the Zn^{2+} ions is responsible for the observed n-type conductivity. We note that most of the FETs fabricated from the intrinsic ZnS NWs do not show any detectable gating effect (data not shown), revealing the importance of the appropriate doping for the construction of high-performance FET devices.

The field-effect mobility (μ_n) and electron concentration (n) of the ZnS:Al NWs can be deduced from their electrical transfer characteristics according to the following equations as:

$$\mu_n = \left(\frac{\mathrm{d}I_{DS}}{\mathrm{d}V_{GS}}\right)\frac{\ln(4h/d)L}{2\pi\varepsilon_0\varepsilon_{SiO_2}V_{DS}} \quad (1)$$

$$n = \left(\frac{\sigma}{q\mu_n}\right) \quad (2)$$

where transconductance $g_m = \mathrm{d}I_{DS}/\mathrm{d}V_{GS}$ is extracted from the linear regime of the I_{DS}–V_{GS} curve, ε_{SiO2} is the dielectric constant of the SiO_2 gate insulator (3.9), L, h, and d represent the NW channel length, gate dielectric thickness, and NW diameter, respectively. σ is the conductivity of the NW and q is elementary charge. Table 1 summarizes the key device parameters of the ZnS:Al NW FETs with varied doping levels. μ_n is estimated to be 0.16 cm^2 V^{-1} s^{-1} for AZ1, while it is enhanced to 0.22 and 18.8 cm^2 V^{-1} s^{-1} for AZ2 and AZ3, respectively. Although the enhancement of μ_n is not in agreement with the conventional assumption that mobility in a semiconductor should decrease with the increase of doping level due to the enhanced carrier scattering, this phenomenon is often observed for the nano-FETs and is likely attributed to the improved electrical contact at a higher doping level.[22] Significantly, n is dominated by the doping level and remarkably increased from 1.9×10^{16} cm^{-3} for AZ1 to 2.18×10^{17} and 1.3×10^{18} cm^{-3} for AZ2 and AZ3, respectively. As a result, the threshold value (V_{th}), which is deduced by extracting the linear portion of the I_{DS}–V_{GS} plot, has also gradually decreased from −8 V for AZ1 to −21 and −30 V for AZ2 and AZ3, respectively, because lower voltage is needed to turn-on the devices at a higher doping level. The above results undoubtedly demonstrate that efficient n-type doping in the ZnS NWs is accomplished by the Al incorporation. Moreover, the electrical transport properties of the NWs could be rationally tuned by adjusting the Al doping level. We note that this n-type doping is very durable; measurements before and after five months give nearly identical results (ESI, Fig. S4†).

The great potential of the ZnS:Al NWs as high-performance UV sensors was exploited, as shown in Fig. 3a. The device was exposed to monochromatic light with varied wavelengths at a constant intensity of 100 μW cm^{-2}. From the wavelength (λ)-dependent I–V curves of the ZnS:Al NW (AZ2), we can see that the conductance of the ZnS:Al NW strongly depends on the light wavelength; the photocurrent is nearly constant (equal to the dark current) at the visible range but increases remarkably with decreasing light wavelength. Fig. 3c depicts the spectral response of the ZnS:Al NW. The cut-off wavelength of ∼330 nm is consistent with the band gap of ZnS, therefore the enhancement of the photocurrent should come from the electron–hole pairs excited by the incident light with energy larger than the band gap.[23] Fig. 3d shows the time response spectra of the ZnS:Al NWs with varied doping levels under pulsed UV light

Table 1 Summary of the key device parameters of the FETs fabricated from ZnS:Al NWs with varied doping levels

Sample no.	V_{th}/ V	g_m/ nS	σ/ S cm^{-1}	μ_n/ cm^2 V^{-1} s^{-1}	n/ $\times 10^{17}$ cm^{-3}
AZ1	−8	0.49	1.5×10^{-3}	0.16	0.19
AZ2	−21	0.7	2.4×10^{-2}	0.22	2.18
AZ3	−30	50.6	3.9	18.8	13

 This journal is © The Royal Society of Chemistry 2012

View Article Online

Published on 28 February 2012. Downloaded by HeFei University of Technology on 18/10/2015 13:13:38.

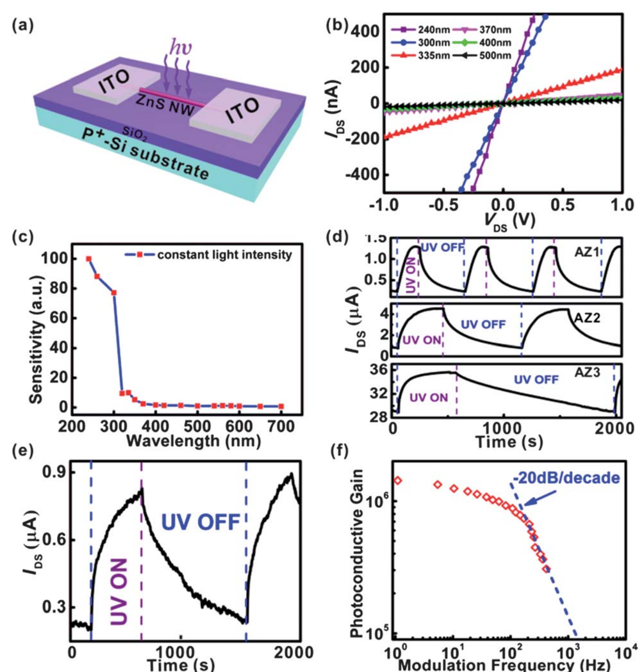

Fig. 3 (a) Schematic illustration shows the configuration for the photoconductive measurement. (b) *I–V* curves of the ZnS:Al NW (AZ2) measured under the light illumination with varied wavelengths at a constant light intensity of 100 μW cm^{-2} and (c) corresponding spectral response of the NW. (d) Time response of the ZnS:Al NWs with varied doping levels at $V_{DS} = +5$ V. UV light (254 nm, 300 μW cm^{-2}) was turned on and off manually. (e) Time response of the ZnS:Al NW (AZ2) measured at a weaker UV light intensity of 5 μW cm^{-2}. (f) Frequency dependence of the photoconductive gain, with an excitation intensity of 100 μW cm^{-2} ($\lambda \approx 254$ nm) and an external applied bias of +5 V.

illumination at $V_{DS} = +5$ V. It is seen that all the devices exhibit excellent stability and reproducibility, while the doping level also significantly impacts the photoconductive properties in terms of photocurrent and response speed.

Responsivity (*R*) is a key parameter for a photodetector and reflects the sensitivity of the photodetector to the incident light. A large *R* is usually desired for practical applications, especially for the weak light detection. *R* can be expressed as:

$$R(\mathrm{A\ W^{-1}}) = \left(\frac{I_P}{P_{opt}}\right) = \eta\left(\frac{q\lambda}{hc}\right)G \quad (3)$$

$$G = \left(\frac{N_{el}}{N_{ph}}\right) = \left(\frac{\tau}{\tau_{tr}}\right) \quad (4)$$

where I_P is the photocurrent, P_{opt} the incident light power, η the quantum efficiency, *h* Planck's constant, *c* the speed of light, λ the incident light wavelength, and *G* the photoconductive gain, which is defined as the ratio between the number of electrons collected per unit time (N_{el}) and the number of absorbed photons per unit time (N_{ph}) or the ratio of carrier lifetime (τ) to carrier transit time (τ_{tr}). Based on the above equations, *R* is estimated to be 8.8×10^5 A W^{-1} for AZ1, 3.1×10^6 A W^{-1} for AZ2, and 4.7×10^6 A W^{-1} for AZ3 at $V_{DS} = +5$ V by assuming $\eta = 1$ for simplification (Table 2). Meanwhile, *G* has also increased from 4.3×10^6 for AZ1 to 1.5×10^7 for AZ2, and to 2.3×10^7 for AZ3.

Table 2 Summary of the photoconductive properties of the ZnS:Al NWs with varied doping levels

Sample no.	*R*/A W^{-1}	*G*	t_r/s	t_f/s
AZ1	8.8×10^5	4.3×10^6	95	209
AZ2	3.1×10^6	1.5×10^7	153	445
AZ3	4.7×10^6	2.3×10^7	203	1185

In contrast, the undoped ZnS NWs exhibit a very weak response to the incident light (data not shown), giving rise to a *R* value lower than 0.3 A W^{-1}. The substantial improvement in *R* and *G* for the ZnS:Al NWs could be ascribed to (i) the high crystal quality of the ZnS:Al NWs and the ohmic contact achieved by ITO electrodes, leading to a large photocurrent; (ii) the separation of the photogenerated electron–hole pairs caused by the surface energy band bending near the NW surface and consequently a longer carrier lifetime;[24] and (iii) Al donors in the ZnS NW may serve as the trapping centres for the holes, thus further prolonging the carrier lifetime. The *R* and *G* values for the ZnS:Al NWs are much higher than previous reports on ZnS films and intrinsic ZnS nanostructures.[25,26] With such high *R* and *G*, it is possible to reach even single-photon detectivity in a single NW.[13] In order to confirm this assumption, light with very low intensity of 5 μW cm^{-2} ($\sim 2 \times 10^{-14}$ W on the NW, corresponding to a photon flux of $\sim 2.5 \times 10^4$ per second) was used (Fig. 3e). It is noted that the NW shows a significant response to the weak light irradiation and also has the potential to detect light with lower intensity. *R* and *G* values are estimated to be 3×10^7 A W^{-1} and 1.5×10^8, respectively, at this light intensity, which are much larger than that at higher light intensity. The decrease of the *R* and *G* at higher light intensity is a manifestation of hole-trapping saturation, *i.e.*, the hole trapping centres are fully occupied, thus leading to the enhancement of the carrier recombination.[13]

From Fig. 3d, it is shown that the response speed of the ZnS:Al NWs to the pulsed light relies on the doping level; more time is needed for the devices to reach the equilibrium at a higher doping level. As shown in Table 2, rise time and fall time (t_r, t_f) are (95 s, 209 s) for AZ1, while the values increase dramatically to (153 s, 445 s) for AZ2, and (203 s, 1185 s) for AZ3. The carrier trapping centres induced by the Al doping might be responsible for this result, which can capture the photogenerated carriers during the light illumination and then slowly release them after the light is turned off, giving rise to the long rise and decay edges.[27] Due to the large dark current at a higher doping level, the I_{light}/I_{dark} ratio decreases from ∼15 for AZ1 to ∼1.5 for AZ3. On the other hand, the response speed is also determined by the light intensity detected. Upon weak light irradiation (Fig. 3e), (t_r, t_f) for AZ2 are (235 s, 676 s), in contrast to the lower values of (153 s, 445 s) measured at higher light intensity. The reduction of the response time with increased light intensity is in good agreement with Rose's model, which assumes that traps are distributed with varying concentration in the band gap.[28,29] The NW was not in a thermal equilibrium state under light illumination, and excess electrons and holes are generated. Correspondingly, two quasi-Fermi levels are induced: one for electrons and another for holes. The quasi-Fermi levels for electrons and holes tend to shift toward the conduction and valence bands, respectively, when the light intensity is increased. As a result, an increasing number of

View Article Online

Published on 28 February 2012. Downloaded by HeFei University of Technology on 18/10/2015 13:13:38.

traps are converted to recombination centres, resulting in shorter rise and fall times.[23] Although the long photocurrent relaxation time for the ZnS:Al NWs may limit their application in high speed optical switches, the large gain values ensure that the devices have a large gain-bandwidth (GB), that is, the devices still have a significant photoresponse even at high modulation frequencies for the incident light. Fig. 4f plots the relationship of G with the modulation frequency (ν), it is seen that the gain values are consistently high even in the millisecond time domain. G is about 2×10^5 at $\nu = 300$ Hz, leading to a large GB value of ~0.1 GHz.[13]

Besides the visible-blind UV sensors, the applications of the ZnS:Al NWs as high-sensitive humidity sensors were further investigated in this work. Fig. 4a shows the I–V curves of the ZnS:Al NW (AZ2) measured at varied RH values ranging from 30% to 90%. When the RH value is beneath 50%, the resistance of the ZnS:Al NW (R_{rh}) slightly increases with increasing RH value, while further increase of the RH value results in an obvious decrease of the resistance. From the semi-logarithmic plots of resistance and sensitivity (R_{air}/R_{rh}) of the ZnS:Al NW *versus* RH value (Fig. 4b), we can see that the sensitivity is nearly proportional to the RH value in the range of 50–90% and a large variation of about 2 orders of magnitude is revealed. This result surpasses previous reports on carbon NT and SnO_2 NW humidity sensors.[15,30] To interpret the resistance increase at RH < 50%, a surface charge transfer model is proposed: due to the chemical adsorption of water molecules, OH^- ions are likely formed on the ZnS:Al NW surface by capturing free electrons from the NW bulk.[31] The surface negative charges make the NW surface energy bands bending upwards (Fig. 4c), hence the holes will accumulate near the surface. A portion of the electrons in NW is compensated by the excess holes, and as a result, the NW resistance increases. In principle, the NW could even be converted to p-type if the chemical absorption of the water molecules is further enhanced, similar to that has been discovered in n-type Si NWs.[31] However, both electrical transfer measurements performed at 30% and 70% RHs show pronounced n-type conduction except the slight increase in the leakage current (I_{GS}), indicating that the physical adsorption instead of the chemical adsorption dominates the conduction and finally contributes to the decrease of the resistance at higher humidity.

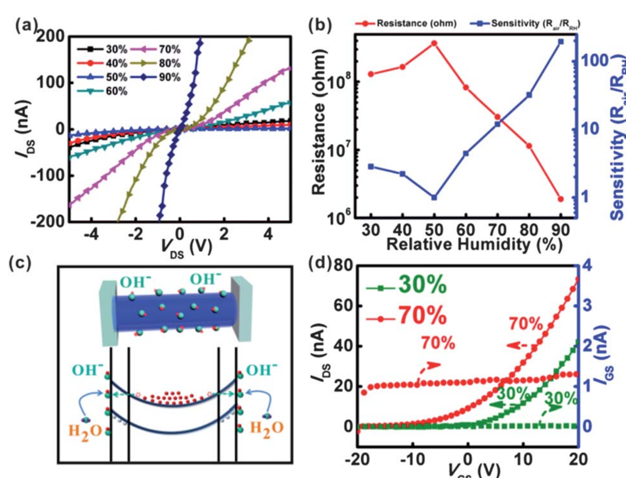

Fig. 4 (a) I–V curves of an individual ZnS:Al NW (AZ2) measured at varied RH values. (b) Semi-logarithmic plots of resistance and sensitivity of the NW *versus* the RH value. (c) Up: schematic illustration shows the adsorption of the water molecules on the NW surface. Down: corresponding energy band diagram of the NW. (d) I_{DS}–V_{GS} and I_{GS}–V_{GS} curves of the NW measured at 30% and 70% RH, respectively.

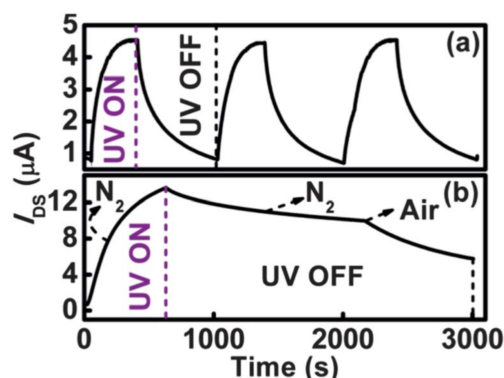

Fig. 5 Time response of the ZnS:Al NW (AZ2) when the NW was exposed to (a) air and (b) a dry N_2 gas flow (200 sccm).

Interestingly, it is found that the humidity is also an important factor that impacts the photoconductive properties of the ZnS:Al NWs, as shown in Fig. 5. In this study, the localized humidity around the NW was changed by blowing the NW with a constant dry N_2 gas flow (200 sccm). The humidity in an ambient environment is ~70% RH and then reduced to ~10% RH under N_2 gas blowing. As compared with the time response measured in ambient humidity (Fig. 5a), the photocurrent of the ZnS:Al NW under N_2 gas blowing increases remarkably, along with the obvious prolongation of the rise and decay edges (Fig. 5b). The increase of the photocurrent at lower humidity could be attributed to the desorption of the water molecules. Water adsorption on the NW surface may reduce the photocurrent by capturing electrons from the NW, which means a "drier" NW should have a higher photocurrent. On the other hand, at ambient humidity, the excess carriers could be quickly captured and recombined due to the adsorption of the water molecules after the light is turned off, hence the decay edge is more steep. In contrast, a permanent photocurrent is observed for the NW in a low RH value because of the longer carrier lifetime. This assumption is examined by shutting off the N_2 gas flow and exposing the NW to the ambient environment again (Fig. 5b). It is clear that the decline of the photocurrent becomes faster in air. Our results demonstrate that the surface effect plays an important role in determining the photoconductive properties of the ZnS:Al NWs.

IV. Conclusions

In summary, Al-doped ZnS NWs with controlled n-type conductivity were successfully synthesized *via* a thermal co-evaporation method. The ZnS:Al NWs were single crystalline with wurtzite structure and $[10\bar{1}0]$ orientation. By adjusting the doping level, the conductivities of the ZnS:Al NWs could be tuned in a wide range of 3 orders of magnitude and a high electron concentration up to 1.3×10^{18} cm^{-3} was achieved. The ZnS:Al NWs could serve as visible-blind UV sensors with an

 This journal is © The Royal Society of Chemistry 2012

Published on 28 February 2012. Downloaded by HeFei University of Technology on 18/10/2015 13:13:38.

extremely high responsivity of 4.7×10^6 A W^{-1} and a large GB of ~0.1 GHz. The potential of the NWs as high-sensitive humidity sensors was further exploited. It is expected that the n-type ZnS NWs will have important applications in the new-generation nanoelectronic and optoelectronic devices.

Acknowledgements

This work was supported by the Major Research Plan of the National Natural Science Foundation of China (no. 91027021), the Program for New Century Excellent Talents in University of the Chinese Ministry of Education (NCET-08-0764), National Basic Research Program of China (973 Program, no. 2012CB932400), and the National Natural Science Foundation of China (NSFC, no. 60806028, 51172151, 20901021, 21101051, 61106010).

Notes and references

1 J. S. Jie, W. J. Zhang, Y. Jiang, X. M. Meng, J. A. Zapien, M. W. Shao and S. T. Lee, *Nanotechnology*, 2006, **17**, 2913.
2 Y. Jiang, W. J. Zhang, J. S. Jie, X. M. Meng, J. A. Zapien and S. T. Lee, *Adv. Mater.*, 2006, **18**, 1527.
3 Y. Jiang, X. M. Meng, J. Liu, Z. Y. Xie, C. S. Lee and S. T. Lee, *Adv. Mater.*, 2003, **15**, 323.
4 S. Farhangfar, R. B. Yang, M. Pelletier and K. Nielsch, *Nanotechnology*, 2009, **20**, 325602.
5 H. Gao, X. T. Zhang, M. Y. Zhou, Z. G. Zhang and X. Z. Wang, *Nanotechnology*, 2007, **18**, 065601.
6 J. S. Jie, W. J. Zhang, I. Bello, C. S. Lee and S. T. Lee, *Nano Today*, 2010, **5**, 313.
7 Z. G. Chen, L. Cheng, H. Y. Xu, J. Z. Liu, J. Zou, T. Sekiguchi, G. Q. M. Lu and H. M. Cheng, *Adv. Mater.*, 2010, **22**, 2376.
8 X. S. Fang, Y. Bando, M. Y. Liao, T. Y. Zhai, U. K. Gautam, L. Li, Y. S. Koide and D. Golberg, *Adv. Funct. Mater.*, 2010, **20**, 500.
9 Y. Q. Yu, J. S. Jie, P. Jiang, L. Wang, C. Y. Wu, Q. Peng, X. W. Zhang, Z. Wang, C. Xie, D. Wu and Y. Jiang, *J. Mater. Chem.*, 2011, **21**, 12632.
10 Rajesh, B. K. Das, S. Srinives and A. Mulchandani, *Appl. Phys. Lett.*, 2011, **98**, 013701.
11 M. J. Ruedas-Rama, A. Orte, E. A. H. Hall, J. M. Alvarez-Pez and E. M. Talavera, *Chem. Commun.*, 2011, **47**, 2898.
12 N. Üzar, S. Okur and M. Ç. Arıkan, *Sens. Actuators, A*, 2010, **167**, 188.
13 C. Soci, A. Zhang, B. Xiang, S. A. Dayeh, D. P. R. Aplin, J. Park, X. Y. Bao, Y. H. Lo and D. Wang, *Nano Lett.*, 2007, **7**, 1003.
14 J. W. Lee, K. J. Moon, M. H. Ham and J. M. Myoung, *Solid State Commun.*, 2008, **148**, 194.
15 Q. Kuang, C. S. Lao, Z. L. Wang, Z. X. Xie and L. S. Zheng, *J. Am. Chem. Soc.*, 2007, **129**, 6070.
16 J. T. W. Yeow and J. P. M. She, *Nanotechnology*, 2006, **17**, 5441.
17 C. Y. Wu, J. S. Jie, L. Wang, Y. Q. Yu, Q. Peng, X. W. Zhang, J. J. Cai, H. Guo, D. Wu and Y. Jiang, *Nanotechnology*, 2010, **21**, 505203.
18 G. D. Yuan, W. J. Zhang, W. F. Zhang, X. Fan, I. Bello, C. S. Lee and S. T. Lee, *Appl. Phys. Lett.*, 2008, **93**, 213102.
19 Q. Peng, J. S. Jie, C. Xie, L. Wang, X. Zhang, D. Wu, Y. Q. Yu, C. Y. Wu, Z. Wang and P. Jiang, *Appl. Phys. Lett.*, 2011, **98**, 123117.
20 X. W. Zhang, J. S. Jie, Z. Wang, C. Y. Wu, L. Wang, Q. Peng, Y. Q. Yu, P. Jiang and C. Xie, *J. Mater. Chem.*, 2011, **21**, 6736.
21 P. Prathap, N. Revathi, Y. P. V. Subbaiah, K. T. Ramakrishna Reddy and R. W. Miles, *Solid State Sci.*, 2009, **11**, 224.
22 G. F. Zheng, W. Lu, S. Jin and C. M. Lieber, *Adv. Mater.*, 2004, **16**, 1890.
23 Y. Jiang, W. J. Zhang, J. S. Jie, X. M. Meng, X. Fan and S. T. Lee, *Adv. Funct. Mater.*, 2007, **17**, 1795.
24 M. Marso, R. Calarco, T. Richter, A. I. Aykanat, R. Meijers, A. v. d. Hart, T. Stoica and H. Lüth, *Nano Lett.*, 2005, **5**, 981.
25 E. Monroy, F. Omnes and F. Calle, *Semicond. Sci. Technol.*, 2003, **18**, 33.
26 X. S. Fang, S. L. Xiong, T. Y. Zhai, Y. Bando, M. Y. Liao, U. K. Gautam, Y. Koide, X. Zhang, Y. T. Qian and D. Golberg, *Adv. Mater.*, 2009, **21**, 5016.
27 J. S. Jie, W. J. Zhang, Y. Jiang, X. M. Meng, Y. Q. Li and S. T. Lee, *Nano Lett.*, 2006, **6**, 1887.
28 N. V. Joshi, *Photoconductivity: Art, Science, and Technology*, Marcel Dekker, New York, 1990.
29 A. Rose, *Concepts in Photoconductivity and Allied Problems*, Krieger, New York, 1978.
30 X. J. Huang, Y. F. Sun, L. C. Wang, F. L. Meng and J. H. Liu, *Nanotechnology*, 2004, **15**, 1284.
31 J. S. Jie, W. J. Zhang, K. Q. Peng, G. D. Yuan, C. S. Lee and S. T. Lee, *Adv. Funct. Mater.*, 2008, **18**, 3251.